EURASIAN PHYSICAL TECHNICAL JOURNAL

2024, Volume 21, No.4 (50)

https://doi.org/10.31489/2024No4/35-48

Received: 20/07/2024 Revised: 13/10/2024 Accepted: 18/12/2024 Published online: 25/12/2024

Original Research Article

UDC 535.37

RADIATION SYNTHESIS OF BARIUM MAGNESIUM FLUORIDE ACTIVATED BY TUNGSTEN CERAMICS: STRUCTURE AND LUMINESCENCE

Lisitsyn V.M.[1], Vaganov V.A.[1], Alpyssova G.K.[2]*, Kaneva E.V.[3], Lisitsyna L.A[4]., Strelkova A.V.[5], Denisov I.P.[1]

[1] National Research Tomsk Polytechnic University, Tomsk, Russia
[2] E.A. Buketov Karagandy University, Karaganda, Kazakhstan
[3] Vinogradov Institute of Geochemistry SB RAS, Irkutsk, Russia
[4] Tomsk State University of Architecture and Building, Tomsk, Russia
[5] L.N. Gumilyov Eurasian National University, Astana, Kazakhstan
*Corresponding author: gulnur-0909@mail.ru

Abstract. *In the work on the example of barium magnesium fluoride activated by tungsten system the existence of possibility of introduction of activators, modifiers into the formed ceramics are shown. Using unique properties of radiation synthesis of high synthesis rate is happened. The possibility of synthesis of magnesium fluoride activated by tungsten, barium fluoride activated by tungsten and barium magnesium fluoride activated by tungsten ceramics by impact on the charge of a stream of electrons with energy 1.4 MeV with power density 15 kW/cm^2 is shown. The X-ray diffraction, photoexcitation and luminescence spectra, integral spectra of pulsed cathodoluminescence and its decay kinetics have shown that during radiation synthesis tungsten centers the crystal lattice of ceramics. The formed volatile compounds of hexafluoride tungsten do not have time to leave the reaction zone during the synthesis. The efficiency of synthesis reaches 99%. Addition of tungsten oxide to the charge in the amount of up to 2% of the total weight does not affect the formation of ceramics*

Keywords: ceramics; luminescence; radiation-assisted synthesis, X-ray diffraction spectra, optical properties of ceramics.

1. Introduction

Prospective scintillators are materials based on alkaline earth and alkali metal fluorides activated by polyvalent ions [1]. Introducing activators into the crystal lattice of these materials is a complex task. Metal fluoride crystals like LiF, MgF_2, and BaF_2 exhibit a high degree of structural perfection. Activators, being polyvalent ions, have difficulty incorporating into the lattice due to differences in charge and size [2]. Therefore, additional elements are introduced to compensate for this difference in order to incorporate the activator ions into the lattice. Facilitating the introduction of activators into crystals can be achieved by creating conditions that distort the lattice and promote the formation of a complex lattice structure. Examples of such crystals include $LiYF_4$ [3, 4], $NaYF_4$ with activators [5, 6], and $NaGdF_4$ [7]. A complex structure is obtained in the synthesis from LiF (NaF) and YF3 (GdF_4) with cubic and rhombohedral symmetries and similar systems [8]. Another possible matrix for obtaining activated material is $BaMgF_4$, which is derived

from BaF2 with a fluorite lattice and MgF_2 with a rutile lattice [9]. Effective activators (modifier) in metal fluoride-based materials include W, U, and Ti ions. However, their introduction into the crystalline lattice is challenging. At high temperatures of a thermal synthesis, fluoride compounds are formed with low melting points: 2.3, 64, 426°C, and boiling points: 17, 56, 285°C for W, U, Ti fluorides, respectively. Activators W, U, Ti are extracted from the melt. Therefore, the synthesis of activated materials based on them is carried out in an oxidative atmosphere, and LiOH is added to the mixture to facilitate the process. The introduction of substances that aid in synthesis into the initial charge affects the properties of the resulting materials.

A promising method for producing ceramics based on refractory materials is radiation synthesis. Radiation synthesis is carried out solely using a radiation energy, from charge materials of stoichiometric composition without additives, and without the use of any materials that facilitate synthesis, within a time frame of less than 1 second, in an air environment [10]. It can be expected that during radiation synthesis, tungsten ions will not have the opportunity to leave the area where ceramic formation occurs and will be incorporated into the lattice. The possibility of using radiation for the synthesis of MgF_2: W ceramics was demonstrated in a study [11]. The results presented in [12] indicate the possibility of obtaining tungsten-activated ceramics based on alkali earth and alkali metal fluorides.

2. Materials and methods

Ceramic synthesis was achieved by direct electron beam irradiation of the initial mixture of a specified composition using the UNU Stand ELV6 accelerator at the Budker Institute of Nuclear Physics, Siberian Branch of the Russian Academy of Sciences. High-energy electron beams with energy of 1.4 MeV were utilized for synthesis. The beam, extracted through a differential pumping system, had a Gaussian cross-sectional shape with an area on the target surface of 1 cm². The synthesis occurs when the threshold power density of the energy flux is exceeded. At the electron energy of 1.4 MeV, electron beams with a power density on the target surface of 15-23 kW/cm² were used for the synthesis of alkaline earth metal fluoride-based ceramics.

A charge of fluorine powders was prepared for synthesizing ceramics of the desired composition. Tungsten oxide powders were added in an amount of 2.0% of the total charge mass for activate the sensitized ceramics. The charge was poured into a massive copper crucible with a surface area of 10x5 cm² and a depth of 7 or 10 mm. The crucible's depth for synthesis was chosen to ensure the complete absorption of the electron beam energy flux by the charge. The crucible was placed on a massive metal table under the accelerator's output orifice. During radiation synthesis, the electron beam was scanned at a frequency of 50 Hz in the transverse direction of the crucible, and the crucible was moved relative to the scanning beam at a speed of 1 cm/s. The total exposure time of the electron beam on the target surface of the charge in the crucible always amounted to 10 seconds, which was due to the design features of the accelerator and the subject table. Since the beam had a size in the target plane of 1 cm², the crucible was moved relative to the scanning beam. Each elementary area of the charge surface was exposed to the action of a 1-second pulse with a rising and falling Gaussian-shaped envelope, lasting 2 ms with a 10 ms period under these conditions.

The samples were synthesized from powders supplied by «Chemreactiv» shops and Hebei Suoyi New Material Technology Co., Ltd. Note that the efficiency of radiation synthesis of alkaline earth metal fluoride ceramics depends on the background of the starting materials. It was shown in [13] that the efficiency of synthesis strongly depends on the size and aspect ratio of the powder particles used for synthesis. Studies on the dispersion of the initial powders used for synthesis to obtain ceramic samples were conducted using laser diffraction with the Shimadzu SALD-7101 laser particle size analyzer. Figure 1 (a, b) provides information on the dispersion composition of the initial materials used for synthesis.

Ceramic synthesis was achieved solely through the energy of radiation flux, using only raw materials without the addition of other facilitating substances. The synthesis resulted in obtaining samples in the form of plates with dimensions similar to the crucible: 10x5 cm². The typical appearance of inactivated and activated W ceramic samples of BaF_2, MgF_2, $BaMgF_4$, synthesized under the influence of an electron beam with E=1.4 MeV, P=15 kW/cm², is shown in Figure 2. Tungsten oxide powder (WO3) was used as an activator. The particle size is given in [14].

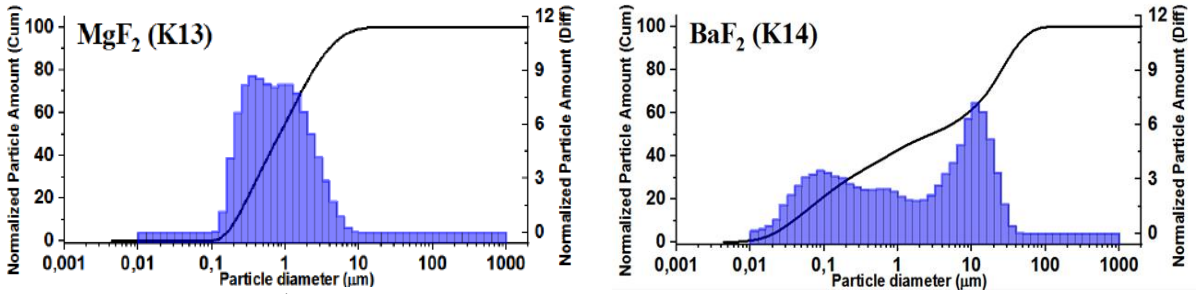

Fig.1. Dispersion composition of MgF_2 (a) and BaF_2 (b) used for powder synthesis.

All samples are solid, glassy and white with shades. The thickness of the samples varies across the area and ranges from 2-4 mm. When struck, the samples shatter like glass. In contrast to solid ceramic materials based on yttrium aluminum garnet, there are no characteristic large voids in the fracture of the described samples, typical of ceramics made of YAG and spinel. The density of the samples of the obtained MgF_2, BaF_2 ceramics is 3.0±0.3 g/cm^3 and 4.8±0.5 g/cm^3, which is close to the density of the corresponding single crystals (3.15 g/cm^3 for MgF_2 and 4.89 g/cm^3 for BaF_2). The surface of the fracture plane is rough, solid. It is worth noting that voids were observed by us earlier during the synthesis of ceramics of alkali-earth metal fluorides from charge materials of different histories. It was assumed that the presence of a significant volume of air in the charge, which does not have time to escape from the reaction zone during the short synthesis time. It is the cause of the void formation inside the synthesized samples. Table 1 provides information on the change in material density during synthesis: the density of the charge used for synthesis ρ_m, the density of the obtained ceramics ρ_{cr} g/cm^3. Here, the density of crystals ρ_{cr} [15] in g/cm^3 is also provided accordingly. The densities of the ceramics obtained by the radiation method were determined with an accuracy of 10%. The sample number in Table 1 represents the experiment number in the system adopted by the authors for record-keeping.

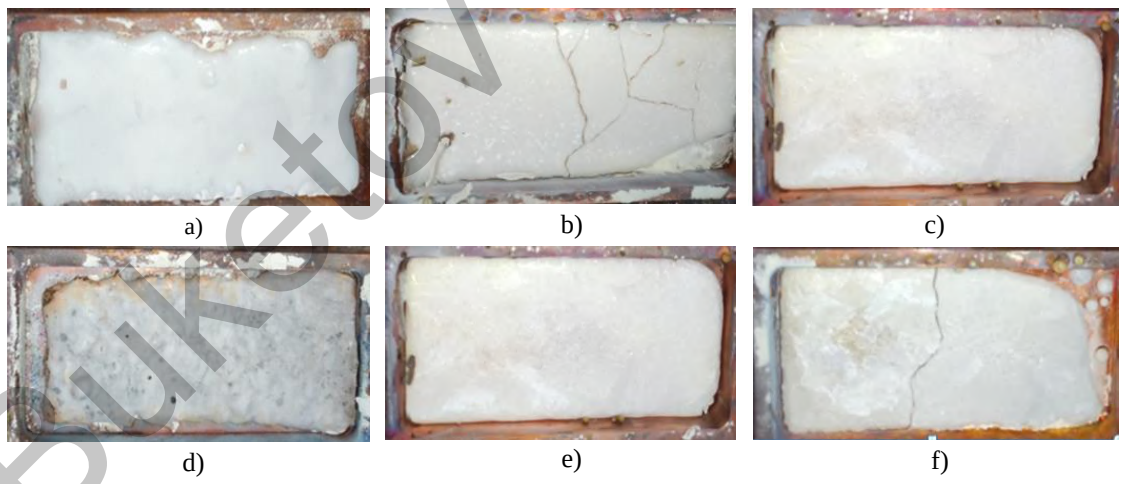

Fig.2. Photos of ceramics samples MgF_2, BaF_2, $BaMgF_4$ (a, b, c), and activated MgF_2:W, BaF_2:W, $BaMgF_4$:W (d, e, f) synthesized under the influence of an electron beam with E=1.4 MeV, P=15 kW/cm^2.

Table 1. Densities of mixture obtained by radiation method of ceramics, crystal in g/cm^3.

No Sample	Composition	ρ_m	ρ_{ce}	ρ_{cr}
516	MgF_2	0.85	2.97	3.15
517	MgF_2:WO_3	0.85	2.97	3.15
519	BaF_2	1.56	4.9	4.89
520	BaF_2:WO_3	1.56	4.8	4.89
521	$BaMgF_4$	1.63	4.5	4.53
522	$BaMgF_4$:WO_3	1.55	4.65	4.53

As can be seen from the results presented in Table 1, the density of the obtained ceramics is equal to the density of the corresponding crystal. The air volume in the BaF_2 and $BaMgF_4$ mixtures is 50% and 70% in MgF_2. However, empty voids are not formed in the ceramics. The same air volumes are present in the mixtures for making ceramics based on YAG, alumina-magnesium spinel, in which voids make up half of the volume.

Table 2 provides information on the synthesis efficiency of the described ceramics when processed with electron beams at an energy of 1.4 MeV and a power density of 15 kW/cm^2. Here, the synthesis efficiency is defined as the ratio of the mass of the synthesized sample to the mass of the charge placed in the crucible.

Table 2. Synthesis efficiency of the studied ceramics.

No Sample	Sample, description	Weight sample, g	Mass loss ΔM, %	Synthesis efficiency
516	MgF_2	42.21	0.40	99.6
517	MgF_2:WO_3	39.26	0.97	99.0
519	BaF_2	66.97	0.75	99.3
520	BaF_2:WO_3	75.9	0.53	99.5
521	$BaMgF_4$	75.71	0.53	99.5
522	$BaMgF_4$:WO_3	75.53	0.56	99.4

As indicated by the presented results, the efficiency of radiation synthesis of ceramics from the used raw materials is very high. The ceramic samples have a weight of up to 75 grams. There are the results of particle distribution based on volume only in figure 1, the relationship between the total volume of particles and their sizes. In MgF_2, the primary range of particle volumes is between 0.2 and 5 micrometers. In BaF_2, the range of particle volumes is much broader, ranging from 0.03 to 30 micrometers. However, the synthesis efficiencies of MgF_2 and BaF_2 ceramics are similar. The quantity of small particles, nano- and sub-micron-sized, in the examined powders is much greater than for micron-sized particles. Nevertheless, their proportion in the overall powder volume is small. Since the synthesis efficiency is 99%, it can be confidently assumed that the ceramics were primarily formed from micron-sized particles. The conclusion is also interesting that ceramics of $BaMgF_4$ are also produced with high efficiency (see Table 2).

3. Results and discussions

3.1. Structure of ceramics

X-ray diffraction patterns were collected using a Bruker D8 ADVANCE (AXS, Berlin, Germany) diffractometer equipped with a scintillation detector. The measurements were performed in step-scan mode over a diffraction angle range (2θ) of 10 to 90° 2θ, employing a CuKα radiation source. The experiments were conducted at room temperature with a flat sample in Bragg-Brentano geometry. The experimental conditions were as follows: 40 kV, 40 mA, exposure time - 2 seconds, step size - 0.02° 2θ. Data processing was conducted using the DIFFRAC plus software package. Sample identification was performed using the Powder Diffraction File (PDF-2) database (ICDD, 2007) and indexing was carried out using the EVA software (Bruker, 2007). The TOPAS 4.2 software package (Bruker, 2008) was used for Rietveld profile fitting, degree of crystallinity, crystallite size and unit cell parameters calculation. Rietveld refinements provided agreement factors, R_{wp}, in the range from 4.9 to 8.4%. The diffraction patterns of the samples (Figures 3-5) have small peaks, indicating the possibility of the presence of certain impurity phases in small quantities.

Figures 3-5 X-ray diffraction pattern of MgF_2 (a) and MgF_2:W (b), BaF_2 (a) and BaF_2:W (b), $BaMgF_4$ (a) and $BaMgF_4$:W (b) samples. The hkl indices of the reflexes of $BaMgF_4$ are marked. Reflections belonging to $BaMgF_4$ and $Ba_6Mg_7F_{26}$ are marked with ◊ and o, respectively.

The results of the study are presented in Table 3 (Appendix). The following data from the PDF-2 database (ICDD, 2007) were used for qualitative phase analysis and indexing of the diffraction patterns:

PDF 01-070-0212 «Magnesium fluoride (MgF_2)», symmetry is tetragonal lattice, space group is *P*42/*mnm* (#136), a = 4.6213 Å, c = 3.0519 Å.

PDF 00-004-0452 «Barium fluoride (BaF_2)», symmetry is face-centered cubic lattice, space group is *Fm–3m* (#225), a = 6.2001 Å.

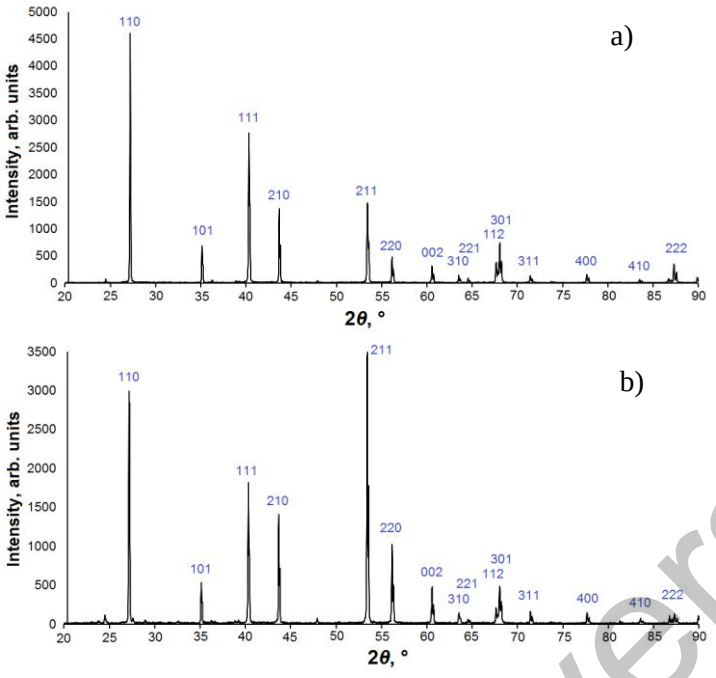

Fig.3. X-ray diffraction pattern of MgF_2 (a) and MgF_2:W (b) samples. The hkl indices of the reflexes of MgF_2 are marked.

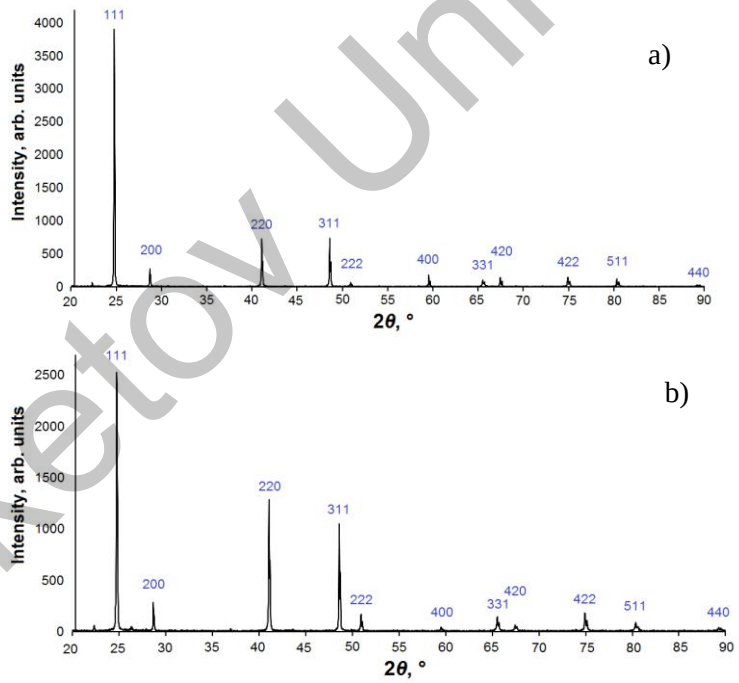

Fig.4. X-ray diffraction pattern of BaF_2 (a) and BaF_2:W (b) samples. The hkl indices of the reflexes of BaF_2 are marked.

PDF 01-087-0201 «Barium magnesium fluoride ($BaMgF_4$)», symmetry – base-centered orthorhombic lattice, space group is *Cmc*21 (#36), $a = 4.126$ Å, $b = 14.518$ Å, $c = 5.821$ Å.

PDF 01-087-0192 «Barium magnesium fluoride ($Ba_6Mg_7F_{26}$)», symmetry is body-centered orthorhombic lattice, space group – *Immm* (#71), $a = 5.8535$ Å, $b = 12.1495$ Å, $c = 15.1109$ Å.

The diffraction patterns of the samples (Figures 3-5) have small peaks, indicating the possibility of the presence of certain impurity phases in small quantities. In all synthesized samples, the dominant phase is the crystalline phase of the corresponding composition, regardless of the presence of tungsten oxide in the charge.

In addition, the precursor phase is detected in all samples. The WO_3 phase is found in MgF_2, BaF_2 is retained along with the $BaMgF_4$ phase. The MgO phase is found in some samples. The appearance of this phase can be explained by oxidation because the synthesis is carried out in an open atmosphere. However, the results of XRD studies show that during radiation treatment, the indicated crystalline phases, including solid solutions, are formed in ceramics.

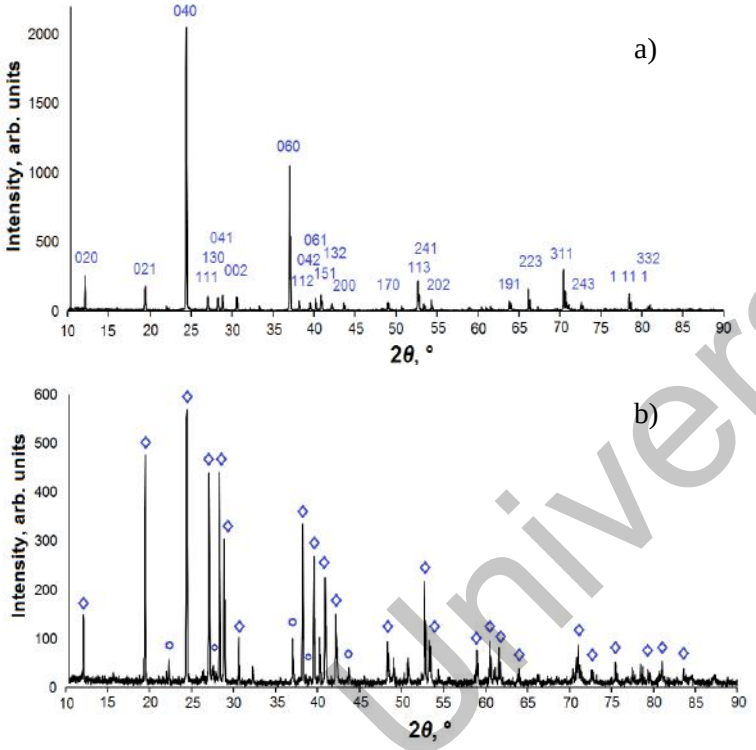

Fig.5. X-ray diffraction pattern of $BaMgF_4$ (a) and $BaMgF_4$:W (b) samples.

Thus, at radiation treatment by powerful flows of high-energy electrons of the charge based on alkaline-earth metal fluorides with tungsten oxide for activation, ceramics with the presence of crystalline phase is formed. Note that the synthesis results depend on the prehistory of the starting substances. The surface microstructure of alkaline earth metal fluorides was studied using a MIRA 3 LMU scanning electron microscope (SEM) (TESCAN). The elemental composition of the samples was obtained using an INCA PentaFET-x3 analyzer (Oxford Instruments, England). To study the surface, a small amount of sample was applied on a conductive carbon tape. A nanometer-thin layer of carbon was applied to the surface of the samples from above by thermal deposition.

The results of composition analysis of synthesized samples of MgF_2, BaF_2, MgF_2:W, BaF_2:W, $BaMgF_4$ and $BaMgF_4$:W fluorides are shown in Fig. 6. In samples MgF_2, BaF_2 the main elements of composition are dominant: Mg, Ba and F. In addition, some amount of oxygen is found in the composition of the ceramic samples. Its presence is explained by the fact that the synthesis is carried out in an open atmosphere, oxygen can enter the pores of the sample. In samples MgF_2:W, BaF_2:W tungsten is detected. We emphasise that tungsten oxide was added to the charge in an amount of 2% of the total mass. The detection of tungsten in ceramics indicates that a significant part of it does not have time to leave the synthesis zone for less than 1 s. and remains in the sample.

Fig. 7 presents SEM images of samples MgF_2:W, BaF_2:W with presentation of the map of distribution of elements by volume. From the presented results it can be seen that part of tungsten is included in the crystallites, but a significant part is concentrated in the intercrystalline space.

As follows from the presented results, the injected activator is distributed very unevenly over the volume of ceramics. The inhomogeneous distribution of the activator is also evident in the measured distribution maps. The main significant conclusion for the method is that after radiation synthesis a part of tungsten was retained in the formed ceramics.

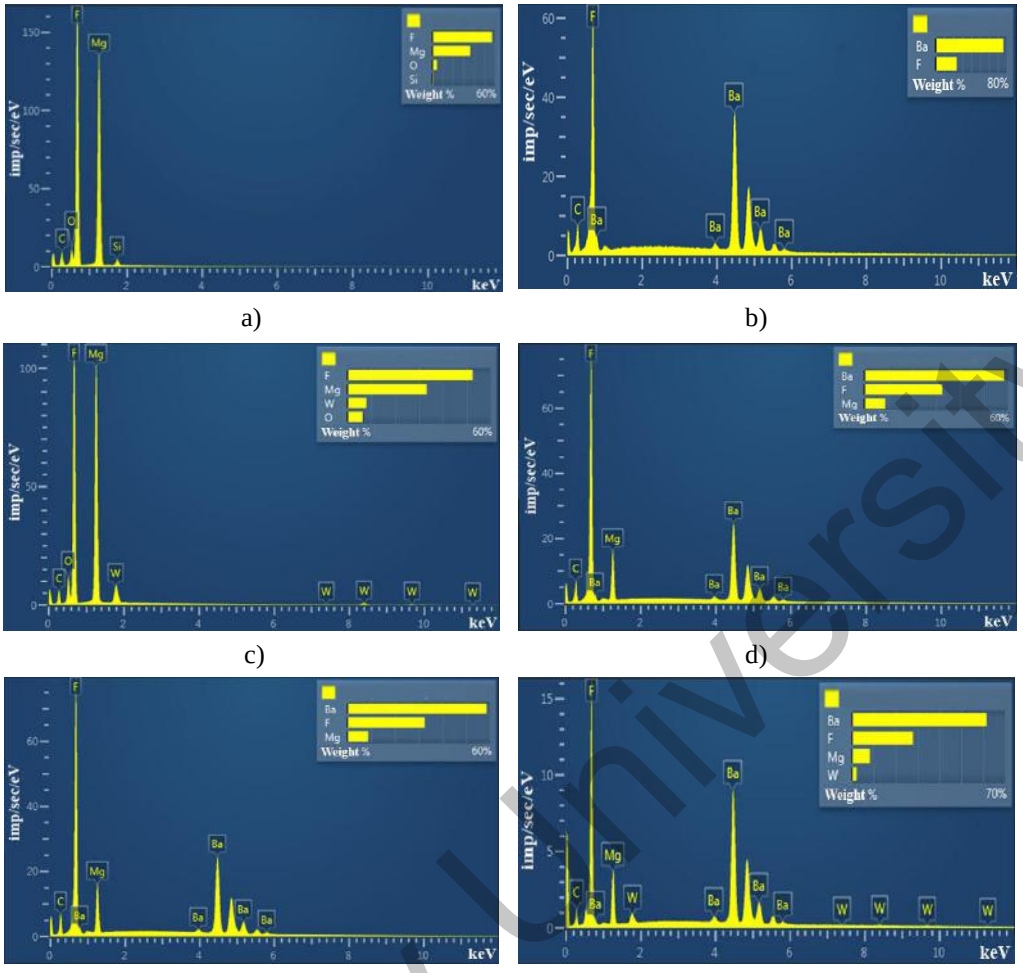

Fig.6. Composition results of MgF_2 (a) and BaF_2 (b) samples (top), MgF_2:W (c), BaF_2:W (d), and $BaMgF_4$ (e), $BaMgF_4$:W (f) (bottom).

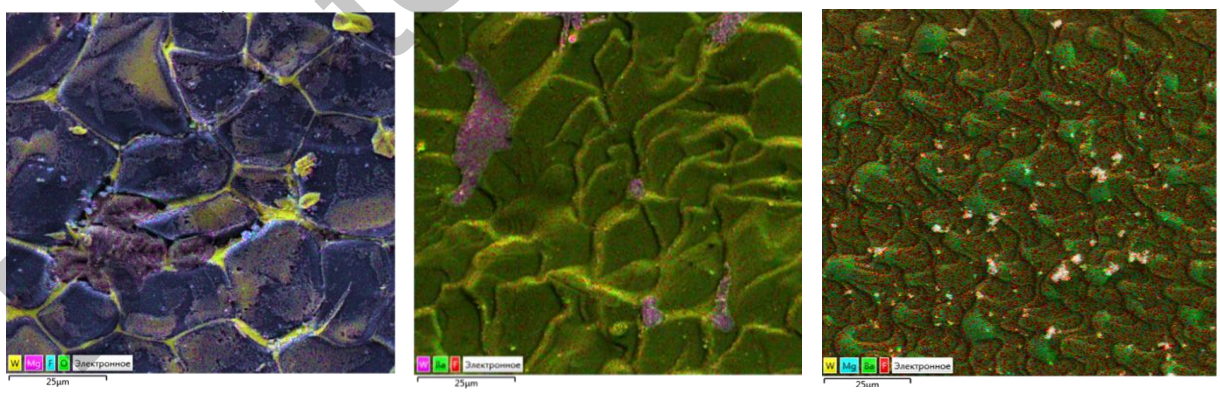

Fig.7. Mappings of the distribution of elements in the samples MgF_2:W (a), BaF_2:W (b), $BaMgF_4$:W (c).

3.2. Luminescence of ceramics

A study cycle of the luminescent properties of tungsten-activated samples of BaF_2, MgF_2 and $BaMgF_4$ synthesized ceramics was carried out, including the spectra of photoexcitation and photoluminescence (PL) under stationary conditions using a SOLAR SM2203 spectrometer. In a summarized form, the spectra are presented in Figure 8.

The figures depict series of luminescence spectra taken from various sections of synthesized ceramic samples. The spectra of all fragments from each sample are similar. Measurements were conducted under identical conditions. Therefore, the presented results can provide an idea of the variation in their intensities over the sample area. We emphasize that the shapes of the bands do not change. In the samples of ceramics synthesized from the charge containing tungsten oxide and without it, the luminescence bands are usually slightly different in position. The luminescence bands in the activated samples are slightly shifted to the long-wave region of the spectrum. The luminescence excitation spectra differ significantly. In non-activated samples luminescence is excited by ultraviolet (UV) radiation in the range from 200 to 260 nm. With the introduction of the activator the excitation band becomes wider. The luminescence is excited by UV radiation in the region up to 300 nm. Changes in the excitation spectra of luminescence and the positions of the bands indicate that with the introduction of tungsten in the crystalline phase of ceramics there is a transformation of the structure of the luminescence centers or, more likely, the local structure in their surroundings. Consequently, tungsten enters the ceramics during synthesis.

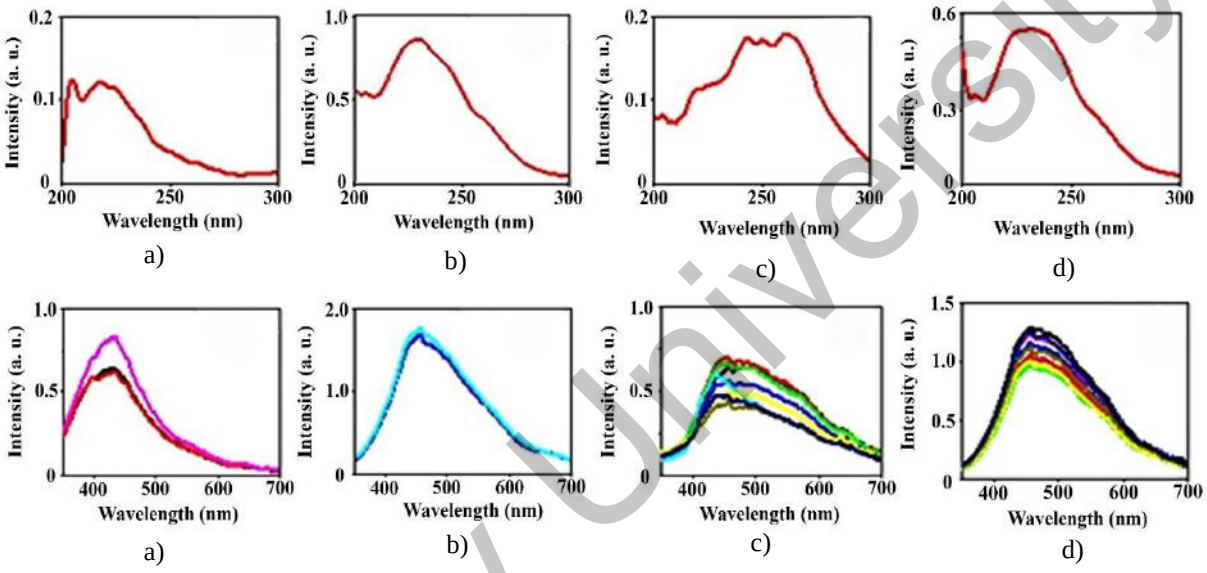

Fig.8. Excitation (top row) and luminescence (bottom row) spectra of $BaMgF_4$ samples (a) when excited at 220 nm, and $BaMgF_4$:W (b), BaF_2:W (c), MgF_2:W3 (d) when excited in the 260 nm range.

Impulse cathodoluminescence (ICL) studies of synthesized ceramic samples have been conducted. An electron accelerator, generating single pulses with the following characteristics, was used as the excitation source for cathodoluminescence: electron energy = 0.25 MeV, pulse duration at half-height = 10 ns, current density at the maximum up to 100 A/cm², and the excitation energy density could vary in the range from 1 to 50 mJ/cm². Luminescence registration was performed using a photomultiplier tube PMT-97 with the use of a monochromator MDR-23 (spectral range 200-2000 nm, linear dispersion 1.3 nm/mm) and a digital oscilloscope Tektronix DPO3034 (300 MHz). Registration of integrated emission spectra of the ICL was carried out using an optical fiber spectrometer AvaSpec-2048 (200 - 1100 nm). The emission spectrum was corrected for the spectral sensitivity of the optical path.

The results of measurements of integrated emission spectra of ICL samples of synthesized ceramics are presented in Fig. 9. The spectra were not normalized for intensity and are presented in a form convenient for comparison. Cathodoluminescence of ceramic samples synthesized from raw materials containing tungsten differs significantly from the luminescence of ceramic samples from raw materials that do not contain tungsten oxide. The cathodoluminescence spectrum of MgF_2: W shows a wide and complex band with a maximum around 570 nm. In ICL spectrum of MgF_2 ceramics, a band with a maximum around 400 nm is observed. In the spectra of ICL of BaF_2 and BaF_2: W ceramics, a band around 390 nm is observed. There is an additional wide band in the range of 520-620 nm in the BaF_2: W spectrum. In the ICL spectrum of $BaMgF_4$ ceramics, a wide band in the range of 400-500 nm is observed, and in $BaMgF_4$: W, the band significantly broadens in the 500-650 nm range. Thus, luminescence in the 520-620 nm range is observed in all ceramic samples synthesized from raw materials containing tungsten oxide.

Some difference of luminescence spectra under photo- and cathode excitation may be due to the following. At optical excitation in PL measurements, the energy is transferred directly to the luminescence center or absorption center with subsequent transfer to the luminescence center. At excitation by high-energy electrons not less than 99% of all absorbed energy of the flux is spent on the creation of electron-hole excitations in the matrix, the created electron-hole excitations transfer energy to the luminescence centers. The influence of the method of excitation energy transfer to the luminescence center can be explained by the complex structure of the luminescence centers, the presence of their own lattice defects in their structure.

The nature of luminescence in tungsten-activated crystals and ceramics of alkaline and alkaline-earth metal fluorides is unknown. However, a significant increase of luminescence intensity by introducing metal ions of tungsten, uranium, titanium into the lattice of metal fluorides is supposed to be promising for obtaining effective scintillators. It should be noted that for introduction of tungsten at thermal synthesis in the charge additionally oxides and hydrides of metals are added. Their introduction contributes to the preservation of tungsten in the reaction zone. Probably, the formation of luminescence centers in the ceramics synthesized by us is promoted by oxygen introduced with tungsten.

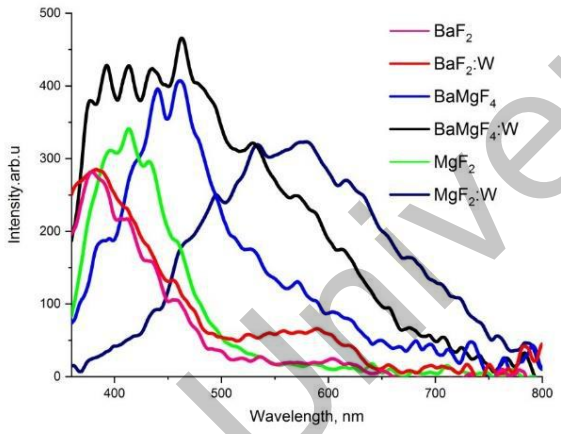

Fig.9. Integral spectra of impulse cathodoluminescence of ceramic samples.

It is possible that oxygen from the environment is involved in the synthesis: the synthesis is carried out in an open atmosphere. Obviously, the active element of the structure of the luminescence centers are anionic vacancies [16], which are always present in metal oxides or as part of anions in the lattice of crystals. Anionic vacancies with trapped electrons in LiF (M centers) are one of the most effective luminescence centers. The assumption that oxygen-vacancy complexes in the crystal lattice can be effective luminescence centers was suggested in [17]. Luminescence of oxygen-vacancy complexes is also observed in other materials, for example, in quartz [18] existing in different phase states [19], in topaz [20, 21], corundum [22], magnesium oxide [23]. Kinetic decay curves after excitation by electron pulses with an energy of 250 keV and a duration of 10 ns were measured. The results of luminescence decay kinetics for BaF_2 and BaF_2:WO_3 are presented in Figure 10.

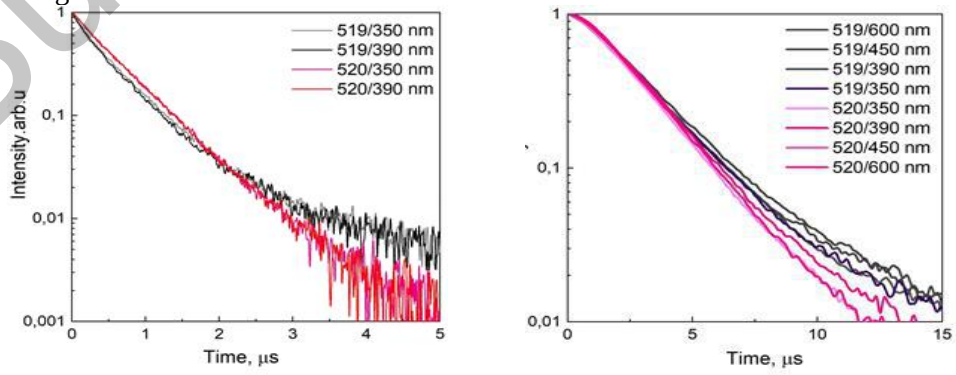

a) b)

Fig.10. Kinetic decay curves of cathodoluminescence for BaF_2 (a) and BaF_2 (b):W

The luminescence spectra are complex and different for all studied ceramic samples. Measurements of kinetic decay curves provide some insight into the change in spectra over time in different spectral regions. The inserts in the figures show sample numbers and the wavelengths of the luminescence spectra at which the measurements were performed. In the time range up to 4 μs, the decay of luminescence in BaF_2: W ceramic samples can be described as a linear function in logarithmic coordinates, while the decay of luminescence in BaF_2 ceramic samples is nonlinear. Differences in kinetic curves over time are also observed for longer times. In the time range of 5-15 μs, the decrease in luminescence intensities is nearly linear in semi-logarithmic coordinates. The rate of luminescence decay in activated ceramic samples is higher than in non-activated ones across the entire measured spectral range (Figure 11).

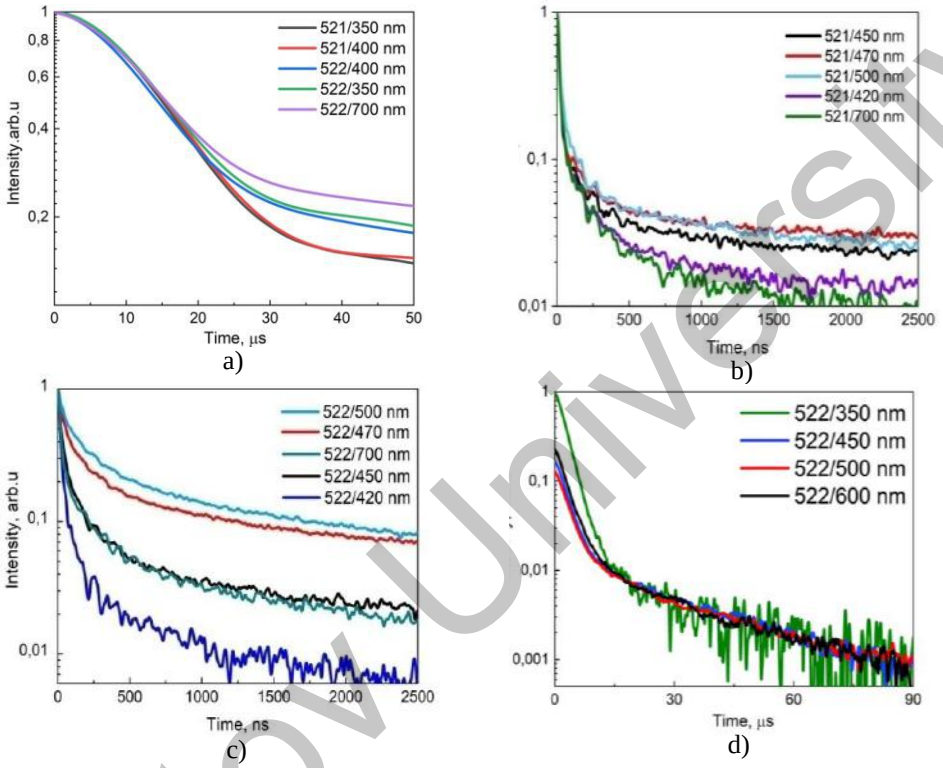

Fig.11. Kinetic decay curves of cathodoluminescence for $BaMgF_4$, BaMgF4:W (a), $BaMgF_4$ (b), BaMgF4:W (c), BaMgF4:W (d) in the nanosecond range.

The decrease in luminescence continues throughout the entire measured spectrum range and within the time range of several microseconds. In the time range of 50 to 500 nanoseconds, a significant difference in the intensity decay of $BaMgF_4$ and $BaMgF_4$:W luminescence is observed in different parts of the spectra, which persist up to 10 microseconds. Thus, the kinetic characteristics of cathodoluminescence in the investigated samples of solid solutions of alkaline earth metal fluorides in activated and non-activated synthesized ceramics are different.

4. Conclusion

Radiation synthesis method for ceramics made from dielectric refractory materials is characterized by high speed, high efficiency, and the absence of the need for additional substances to form new phase structures. The development and establishment of this method are currently in the process of exploring its potential for expanding the range of ceramics that can be synthesized through radiation methods, studying the dependence of synthesis efficiency on radiation processing parameters, the properties of the starting materials for synthesis, and the nature of the processes that facilitate ceramic formation in the presence of intense radiation flux. In this study, using the example of the $Ba_xMg_{(2-x)}F_4$:W system, it is demonstrated that it is possible to introduce activators and modifiers into the forming ceramics, leveraging the unique qualities of radiation synthesis.

The possibility of synthesizing MgF_2 and BaF_2 ceramics by directly exposing the material to an electron beam with an energy of 1.4 MeV and a power density of 15 kW/cm² has also been shown. Samples with

dimensions of up to 10x5x0.4 cm³ and weights of up to 40 g (MgF_2) and 70 g (BaF_2) have been obtained. The density of the synthesized ceramic samples is 3.0±0.3 g/cm³ and 4.8±0.5 g/cm³, which is equivalent to the density of the corresponding single crystals. In cross-section, the samples are solid and do not contain voids, as observed in YAG ceramics [10]. The efficiency of synthesis, defined as the ratio of the mass of the ceramic sample to the mass of the row charge, depends on the characteristics of the starting materials used, primarily their particle size distribution [14]. When using powders of MgF_2 and BaF_2 for synthesis with particle sizes of 0.2-4 μm and a peak distribution at ~0.8 μm and 0.04-25 μm with a peak distribution at ~10 μm, the synthesis efficiency reaches 99%. Adding tungsten oxide (WO_3) to the charge in an amount of up to 2% of the total weight does not affect the formation of MgF_2:W and BaF_2:W ceramics.

Ceramics with complex compositions, such as $BaMgF_4$ and $BaMgF_4$:W, are also efficiently formed in the presence of intense radiation flux, with densities comparable to those of crystals. It appears that the particle size distribution functions of the used powders are sufficient to avoid the creation of local non-stoichiometry during the formation of the crystalline phase. The X-ray diffraction patterns of $BaMgF_4$:W ceramics, attributed to $BaMgF_4$ phase lines with local non-stoichiometry $Ba_6Mg_7F_{26}$, have very low intensity.

Ceramic materials are highly defective. Their luminescence upon excitation is mainly due to the presence of defects in the crystal lattice and impurities. Synthesizing ceramics with activators leads to changes in their luminescent properties. Research has shown that adding tungsten oxide (WO_3) to the charge for ceramic synthesis in amounts up to 2% does not affect synthesis efficiency but results in changes in luminescent properties. The excitation and emission spectra are altered, with shifts towards longer wavelengths. When excited by nanosecond electron beam pulses with an energy of - 0.25 MeV, the ceramic samples exhibit luminescence with specific properties. In the integrated spectra of samples synthesized from charges with WO_3, shifts or new bands in the long-wavelength region are observed. In MgF_2:W, BaF_2:W, and $BaMgF_4$:W ceramics, luminescence in the 450-700 nm range appears.

The luminescence decay kinetics after excitation by nanosecond electron beam pulses also vary. Up to 4 μs, the luminescence decay of BaF_2:W ceramics follows a linear function in logarithmic coordinates, whereas the decay of BaF_2 luminescence is nonlinear. Differences in the kinetic curves are observed even at longer times. In activated samples, the linear decay range in the 5-25 ns range in semi-logarithmic coordinates is wider than in $BaMgF_4$, and the intensity decay is greater. In the 50-500 ns range, significant differences in the intensity decay magnitude between $BaMgF_4$ and $BaMgF_4$:W are observed in various parts of the spectra, which persist up to 10 μs.

The combination of the results of the studies on ceramics synthesized from alkali-earth metal fluorides allows the conclusion that it is possible to introduce tungsten into the ceramic lattice during synthesis in the presence of intense radiation flux. Tungsten does not have time to leave the synthesis zone during the short synthesis time and remains in the lattice.

Conflict of interest statement

The authors declare that they have no conflict of interest in relation to this research, whether financial, personal, authorship or otherwise, that could affect the research and its results presented in this paper.

CRediT author statement

Alpyssova G.K., **Lisitsyn V.M.:** Conceptualization, Data Curation, Writing Original Draft, Supervision**; Vaganov V.A.:** Visualization, Methodology; **Kaneva E.V.:** Formal analysis, Investigation; **Lisitsyna L.A.:** Writing Review & Editing, Supervision; **Strelkova A.:** Writing – Review & Editing, Validation; **Denisov I.P.:** Investigation.
The final manuscript was read and approved by all authors.

Funding

This research has been funded by TPU and INP SB RAS under the project of the Russian Science Foundation of the Russian Federation. (Grant No. 23-73-00108)

Acknowledgements

Work on the study of morphology, photoluminescence, SEM was carried out by in E.A. Buketov Karaganda University under the project of the Science Committee of the Ministry of Science and Higher Education of the Republic of Kazakhstan (Grant No. AP19579177).

References

1 Atroshchenko L.V., Burachas S.F., Gal'chinetskii L.P., Grinev B.V., Ryzhikov V.D., Starzhinskiy N.G. (1998) Kristally scintilljatorov i detektory ionizirujushhih izluchenij na ih osnove [Scintillator crystals and detectors of ionizing radiations on their base]. *Naukova dumka*, 312 Available at: www.irbis-nbuv.gov.ua/cgi-bin/irbis64r_81/cgiirbis_64.exe?Z21ID=&I21DBN=REF&P21DBN=REF&S21STN=1&S21REF=10&S21FMT=fullw [in Russian].

2 Fumiya N., Takumi K., Go O., Naoki K., Noriaki K., Kentaro F., Takayuki Y. (2018) Scintillation, Dosimeter and Optical Properties of MgF2 Transparent Ceramics Doped with Gd3+. *Mater. Res. Bull.*, 98, 83–88. DOI: 10.1016/j.materresbull.2017; 09: 058.

3 Renfro G., Halliburton L., Sibley W., Belt R. (2000) Radiation Effects in LiYF4. *J. Phys. C Solid State Phys.*, 13, 1941. DOI: 10.1088/0022-3719/13/10/013.

4 Morato S.P., Macedo T.C. (1983) F and photochromic Centers in LiYF4: Nd Crystals *Radiat. Eff.*, 72, 229–235. DOI: 10.1080/00337578308218647.

5 Wang M., Mi C.C., Wang W.X, Liu C.H.Y., Wu F., Xu Z.R., Mao C.B., Xu S.K. (2009) Immunolabeling and NIR-excited fluorescent imaging of hela cells by using NaYF4:Yb, Er upconversion nanoparticles. *ACS Nano.*, 3, 1580-1586. DOI: 10.1021/nn900491j.

6 Li Z.Q., Zhang Y., Jiang S. (2008) Multicolor core/shell-structured upconversion fluorescent nanoparticles. *Adv. Mater*., 20, 4765–4769. DOI: 10.1002/adma.200801056.

7 Ma J.J., Zhu W.J., Lei L., Deng D.G., Hua Y.J., Yang Y.M., Xu S.Q., Prasad P.N. (2021) Highly efficient NaGdF4:Ce/Tb nanoscintillator with reduced afterglow and light scattering for high-resolution X-ray imaging. *ACS Appl. Mater. Interfaces*, 13, 44596–44603. DOI: 10.1021/acsami.1c14503.

8 Yang B., Yin L.X., Niu G.D., Yuan J.H., Xue K.H., Tan Z.F., Miao X.S., Niu M., Du X.Y., Song H.S. Lifshitz E., Tang J. (2019) Lead-free halide Rb2CuBr3 as sensitive X-ray scintillator. *Adv. Mater.*, 31, 1904711. DOI: 10.1002/adma.201904711.

9 Buchter S., Fan T., Liberman V., Zayhowski J., Rothschild M., Mason E., Cassanho A., Jenssen H., Burnett J. (2001) Periodically Poled BaMgF4 for Ultraviolet Frequency Generation. *Opt. Lett.*, 26, 1693–1695. DOI:10.1364/OL.26.001693.

10 Lisitsyn V., Mussakhanov D., Tulegenova A., Kaneva E., Lisitsyna L., Golkovski M., Zhunusbekov A.M. (2023) The Optimization of Radiation Synthesis Modes for YAG:Ce Ceramics. *Materials*, 16, 3158. DOI: 10.3390/ma16083158.

11 Karipbayev Zh., Alpyssova G., Mussakhanov D., Kukenova A., Tulegenova A. (2020) Time-resolved luminescence excited with N_2 laser of YAG:CE Ceramics formed by electron beam assisted synthesis. *Eurasian Physical Technical Journal*, 17, 73 – 76. DOI: 10.31489/2020NO1/73-76.

12 Lisitsyn V., Golkovski M., Lisiysyna L., Dauletbekova A., Mussakhanov D., Vaganov V., Tulegenova A., Karipbayev Z. (2019) MgF_2-Based Luminescing Ceramics. *Russ. Phys.J.*, 61. DOI: 10.1007/s11182-019-01617-y.

13 Lisitsyn V., Polisadova E., Lisitsyna L., Tulegenova A., Denisov I., Golkovski M. (2023) Efficiency Dependence of Radiation-Assisted Ceramic Synthesis Based on Metal Oxides and Fluorides on Initial Powder Particle Sizes. *Photonics*, 10: 1084. DOI: 10.3390/photonics10101084.

14 Alpyssova G., Lisitsyn V., Bakiyeva Zh., Chakin I., Kaneva E., Afanasyev D., Tussupbekova A., Vaganov V., Tulegenova A., Tuleuov S. (2024) Characterization of ZnWO4, MgWO4, and CaWO4 Ceramics Synthesized in the Field of a Powerful Radiation Flux. *Ceramics*, 7, 1085-1099. DOI: 10.3390/ceramics7030071.

15 Gingl F. (1997) $BaMgF_4$ and $Ba_2Mg_3F_{10}$: New Examples for Structural Relationships Between Hydrides and Fluorides. Z. Anorg. *Allg. Chem*., 623, 705–709. DOI: 10.1002/zaac.199762301112.

16 Kotomin E.A., Popov A.I. (1998) Radiation-induced point defects in simple oxides. *Nuclear Instruments and Methods in Physics Research B*, 141 (1), 1-15. DOI: 10.1016/S0168-583X(98)00079-2.

17 Lisitsyna L., Lisitsyn V. (2013) Composition Nanodefects in Doped Lithium Fluoride Crystals. *Phys. Solid State*, 55. DOI: 10.1134/S1063783413110139.

18 Garmysheva T., Shendrik R., Paklin A., Shalaev A., Kaneva E., Nepomnyashchikh A. (2022) Luminescence of Oxygen-Deficient Centers in Quartz Glasses. *Glass Phys. Chem.*, 48, 232–235. DOI: 10.1134/S1087659622030038.

19 He J., Jusnes K.F., Tangstad M. (2021) Phase transformation in quartz at elevated temperatures. *Aspects Min Miner Sci.*, 6(1), 691 – 698. DOI: 10.31031/AMMS.2021.06.000629.

20 Bernal R., Souza D., Valerio M., Cruz-Vázquez C., Barboza-Flores M. (2006) Optically Stimulated Luminescence Dosimetry Performance of Natural Brazilian Topaz Exposed to Beta Radiation. *Radiat. Prot. Dosimetry*, 119, 161–163. DOI: 10.1093/rpd/nci677.

21 Priest V., Cowan D., Yasar H., Ross F. (1991) ESR, Optical Absorption, and Luminescence Studies of the Peroxy-Radical Defect in Topaz. *Phys. Rev. B Condens. Matter.*, 44, 9877–9882. DOI: 10.1103/PhysRevB.44.9877.

22 Surdo A., Pustovarov V.A., Kortov V., Kishka A., Zinin E. (2005) Luminescence in Anion-Defective α - Al_2O_3 Crystals over the Nano-, Micro- and Millisecond Intervals. *Nucl. Instrum. Methods Phys. Res. Sect. -Accel. Spectrometers Detect. Assoc. Equip*., 543, 234–238. DOI: 10.1016/j.nima.2005.01.189.

23 Nikiforov S., Lisitsyn V., Ananchenko D.V., Kasatkina Y.P, Golkovski M.G., Ishchenko A. (2022) Luminescent and Dosimetric Properties of Magnesium Oxide Ceramics Synthesized by a High-Energy Electron Beam. *Tech. Phys. Lett.*, 48(6):8. DOI: 10.21883/TPL.2022.06.53454.19174.

AUTHORS' INFORMATION

Lisitsyn, Victor M. – Doctor of Physical and Mathematical Sciences, Professor, Department of Materials Science, National Research Tomsk Polytechnic University, Tomsk, Russia; Scopus Author ID: 35577898600, https://orcid.org/0000-0002-2075-4796; lisitsyn@tpu.ru

Vaganov, Vitalii A. – Master (Eng.), Researcher, Department of Materials Science, Engineering School, National Research Tomsk Polytechnic University, Tomsk, Russia; Scopus Author ID: 56545484700; https://orcid.org/0000-0002-4644-9095; nba_vitas@mail.ru

Alpyssova, Gulnur K. – PhD, Associate Professor, Department of Radiophysics and Electronics, E.A. Buketov Karaganda University, Karaganda, Kazakhstan; Scopus Author ID: 57204979025, https://orcid.org/0000-0002-7164-2188; gulnur-0909@mail.ru

Kaneva, Ekaterina V. – PhD, Candidate of Geological and Mineralogical Sciences, Senior Researcher, X-ray Analysis Laboratory, Vinogradov Institute of Geochemistry SB RAS, Irkutsk, Russia. Scopus Author ID: 54883446000; https://orcid.org/0000-0001-7155-6784; kev604@mail.ru

Lisitsyna, Liudmila A. – PhD, Professor, Department of Physics, Chemistry and Theoretical Mechanics, Tomsk State University of Architecture and Building, Tomsk, Russia; Scopus Author ID: 6602905153; lisitsyna@mail.ru

Denisov, Igor P. – Researcher, Department of Materials Science, National Research Tomsk Polytechnic University, Tomsk, Russia. Scopus AuthorID: 58713871500; dip@tpu.ru

Strelkova, Assel – Master (Sci.), Department of Technical Physics, L.N. Gumilyov Eurasian National University, Astana, Kazakhstan; Scopus Author ID:: 696600x0, https://orcid.org/0000-0002-8437-811X; a.strelkova@nurorda.kz

Appendix

Table 3. The results of the phase composition investigation.

Sample	Main Phase	Degree of crystallinity	Crystallite size	Cell parameters from database	Refined cell parameters
MgF_2	MgF_2	99.9 (±5) %	413 (±25) nm	PDF 01-070-0212(MgF_2), *P*42/*mnm* (#136), *a* = 4.6213 Å, *c* = 3.0519 Å.	*P*42/*mnm*, *a* = 4.620(5) Å, *c* = 3.050(6) Å, *V* = 65.1(1) Å^3
MgF_2: WO_3	MgF_2	99.6 (±5) %	296 (±35) nm	PDF 01-070-0212(MgF_2), *P*42/*mnm* (#136), *a* = 4.6213 Å, *c* = 3.0519 Å.	*P*42/*mnm*, *a* = 4.619(6) Å, *c* = 3.050(6) Å, *V* = 65.1(1) Å^3
BaF_2	BaF_2	99.9 (±5) %	221 (±22) nm	PDF 00-004-0452 (BaF_2), *Fm–3m* (#225), *a* = 6.2001 Å.	*Fm–3m*, *a* = 6.230(5) Å, *V* = 241.8(1) Å^3
BaF_2:WO_3	BaF_2	99.9 (±5) %	123 (±10) nm	PDF 00-004-0452 (BaF_2), *Fm–3m* (#225), *a* = 6.2001 Å.	*Fm–3m*, *a* = 6.228(4) Å, *V* = 241.6(1) Å^3
$BaMgF_4$	$BaMgF_4$	99.9 (±5) %	92 (±15) nm	PDF 01-087-0201 ($BaMgF_4$), *Cmc*21 (#36), *a* = 4.126 Å, *b* = 14.518 Å, *c* = 5.821 Å.	*Cmc*21, *a* = 4.136(7) Å, *b* = 14.490(5) Å, *c* = 5.830(7) Å, *V* = 349.4(1) Å^3
$BaMgF_4$:WO_3	$BaMgF_4$	89.2 (±5) %	87 (±11) nm	PDF 01-087-0201 ($BaMgF_4$), *Cmc*21 (#36), *a* = 4.126 Å, *b* = 14.518 Å, *c* = 5.821 Å.	*Cmc*21, *a* = 4.134(6) Å, *b* = 14.490(3) Å, *c* = 5.827(7) Å, *V* = 349.0(2) Å^3
	$Ba_6Mg_7F_{26}$		352 (±44) nm	PDF 01-087-0192 ($Ba_6Mg_7F_{26}$), *Immm* (#71), *a* = 5.8535 Å, *b* = 12.1495 Å, *c* = 15.1109 Å.	*Immm*, *a* = 5.825(6) Å, *b* = 12.159(10) Å, *c* = 15.147(13) Å, *V* = 1072.8(9) Å^3